Hypersonic Vehicle Inlet Computational Analysis

Dora E. Musielak

University of Texas at Arlington
dmusielak@uta.edu

Abstract

A computational simulation of a M10 scramjet inlet was carried out to assess the performance of a missile as a base for design optimization. Using NASA's VULCAN code, the computational model provided sufficient detail on the flow characteristics and the compression performance at different flight conditions. We found that the inlet design must be optimized for the Mach 10 scramjet missile. The upstream fuel injector could be positioned on the top surface (cowl), a few centimeters upstream from the shock impingement zone. At that point, the cold fuel would transfer the heat away from the wall and, at the same time should mix with the hot air before entering the combustor and igniting.

Keywords: scramjet inlet, high-speed air-breathing propulsion

1 Introduction

Inlets for hypersonic vehicles present the ultimate design challenge. Although geometrically simple, scramjet inlets generate a complicated flow field characterized by the presence of complex flow dynamics such as corner flow, shock-induced separation, and shock/shock/shock-boundary layer interactions. The high local pressure gradients and high heating that results from those interactions influence the aerodynamic and structural design of the overall vehicle. Ultimately, the inlet must be designed to provide efficiently compressed, supersonic flow at the entrance of the combustor.

The interaction between a shock and a boundary layer depends on whether the boundary layer is laminar or turbulent. In the former case the pressure rise through the shock will propagate farther upstream and downstream (the shock will look weaker). On the other hand, the turbulent boundary layer carries more momentum and can better overcome the strong adverse pressure gradients. The internal flow is complex, and the heat environment is harsh. Thick, hot boundary layers are usually present on the compression surfaces of hypersonic inlets.

An initial inviscid flow assessment was carried out to study the internal aerodynamics of a generic two-dimensional 2-m scramjet inlet at several flight Mach number conditions.[1] This preliminary analysis was deemed necessary to first assess the nature and structure of the internal flow interactions and shock structure, and to compare the CFD results using VULCAN with those reported in the literature. That analysis was followed by a full solution of the Navier-Stokes equations to simulate the effects of viscous flow on the inlet, assuming adiabatic walls.

The full-scale generic scramjet inlet consisted of a 11° half angle centerbody spike of 0.4 m diameter, protruding 1 meter from the cowl lip, as shown in Fig. 1. The projected frontal area of the inlet was A_i = 1.76 m^2, and the annulus above the centerbody (internal compression inlet) was 0.8 m. Because the inlet configuration was symmetric, only one half of the inlet was considered; i.e., half the centerbody spike (compression body) and the upper cowl are shown. A 2-block computational grid was used to span the domain.

This condition is representative of a Mach 10 missile scramjet. The shock impinges upon the cowl, inside the internal compression section, at a point closer to end of the computational domain. The bow shock had a shallow angle, $\theta_w \sim 17.7°$. The flow characteristics of this inlet are reported in Ref. 1.

Because the flow at the exit of the inlet and through the isolator determines the performance of the scramjet combustor, it is important to establish the correct geometry and devise an effective grid. A follow up analysis of the scramjet inlet was later reported,[2] using two axisymmetric inlets operating at the same nominal Mach 10 flight condition, but one half the size of the baseline inlet reported above. Thus, the axisymmetric form of the governing Navier-Stokes equations were solved for this part of the analysis. The computational tools used are described elsewhere.[3]

2. Physical Model and Boundary Conditions

The baseline scramjet inlet illustrated schematically in Fig. 1 consists of an 11° half-angle centerbody spike protruding 1 meter from the cowl lip. The projected frontal area of the inlet is A_i = 1.76 m^2. A second inlet is also evaluated. It has the same geometry but is half the size, as compared with the baseline concept. The two cases assumed viscous turbulent flow, and isothermal wall boundary condition was imposed, with T_w = 300 K (see Table 1). The absolute viscosity of air was calculated with Sutherland's relationship, which is a function of the gas temperature.

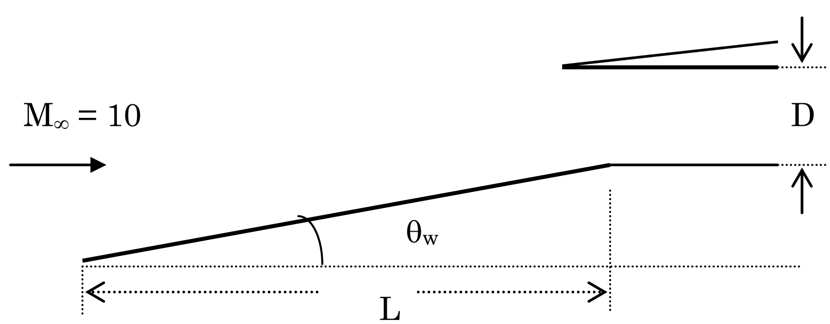

Figure 1. Schematic of Hypersonic Inlet.

Table 1. Scramjet Inlet Flow Conditions

CASE	M_∞	T_∞ (K)	P_∞ (Pa)	Re/m	Inlet L (m)	Isolator D (m)
1	10	225.6	1367.9	4.32 x 10^6	1.0	0.4
2	10	225.6	1367.9	4.32 x 10^6	0.5	0.2

For this inlet configuration, the bow shock forms a shallow angle. Thus, the shock impinges upon the cowl, and it is reflected down into the isolator (entrance to combustion chamber). The shock impinging on the wall causes the gas temperature to increase in this region. This is illustrated with the pressure and temperature contours in Figs. 2 and 3, respectively.

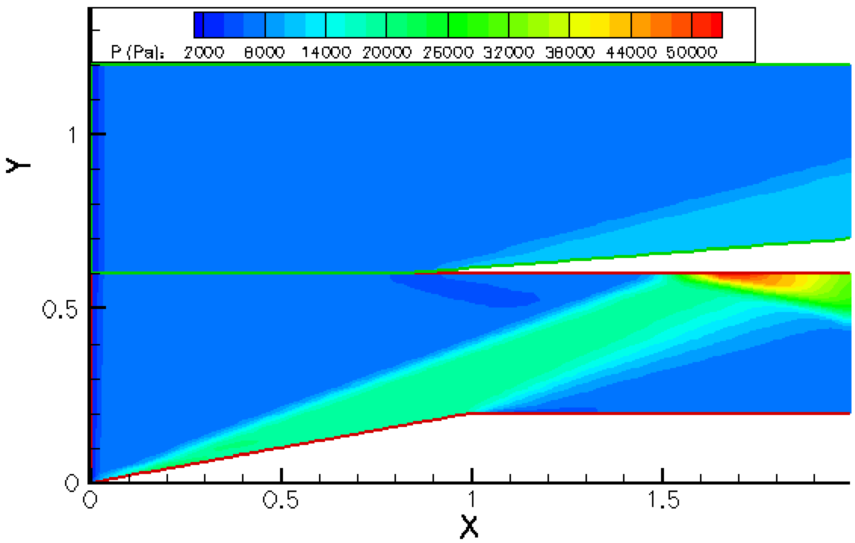

Figure 2. Pressure Field in Long Inlet – Case 1.

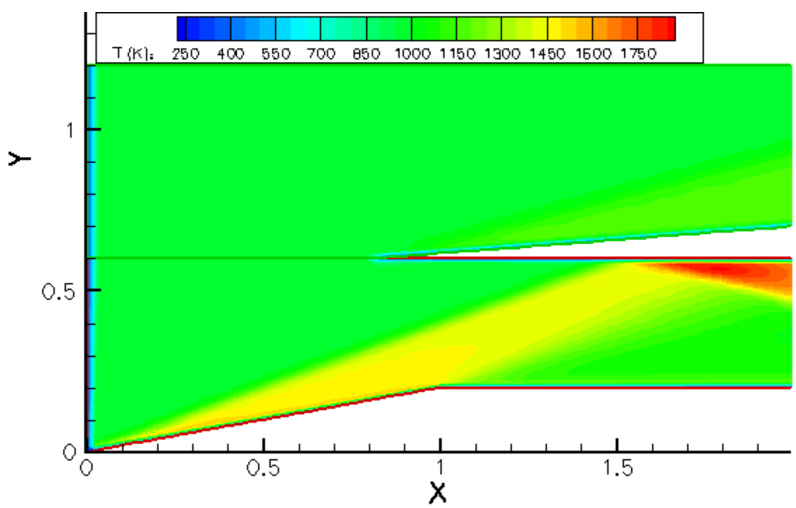

Figure 3. Temperature Field in Long Inlet – Case 1.

The baseline long inlet performed better than the short inlet. Figures 4 and 5 show the radial distribution of axial velocity, pressure, temperature, and Mach number at the exit plane of the long inlet. As shown, the gas left the isolator at a fairly uniform condition, except in the region closer to the upper wall where the shock interacted with the turbulent boundary layer. Overall, this inlet provided a compression ratio of 4.66 and a temperature ratio of 4.67 (measured at the half plane of the isolator). No boundary layer separation was observed. The shorter inlet did not provide the desired gas compression, and thus it is not adequate for operation at this flight condition.

As shown in Fig. 4, the axial velocity profile is fairly smooth; however the Mach number curve shows a gradual decrease in magnitude and then a sudden drop before going to zero at the upper wall. This is the result of the rapid increase in temperature and pressure in the region where the shock interacts with the boundary layer.

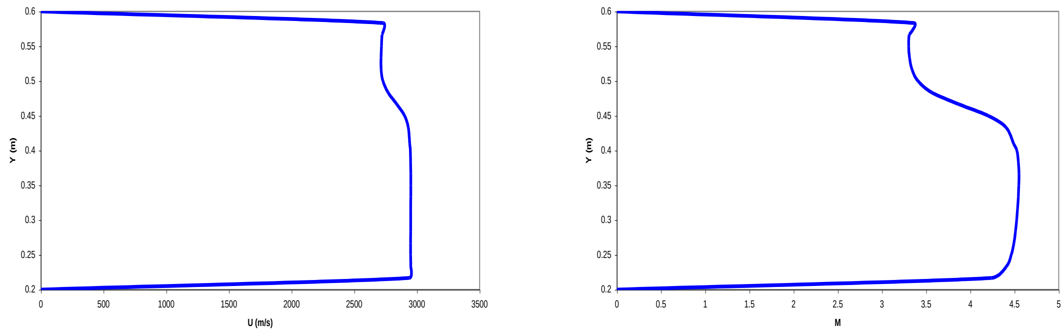

Figure 4. Radial Distribution of Velocity and Mach Number – Long Inlet Case 1.

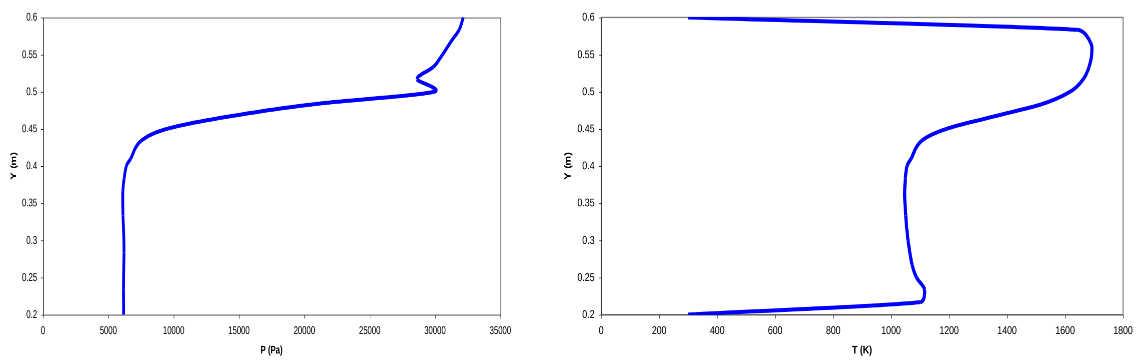

Figure 5. Pressure and Temperature Distribution at Exit Plane – Long Inlet Case 1.

Finally, Fig. 6 gives the wall pressure distribution along the centerbody. The first peak of the curve indicates the shock developing over the nose, and the dipping of the profile indicates the flow turning downstream from the corner at $x = 1$ m.

Overall, the performance of this inlet is excellent. No indication of boundary layer separation was observed, even in the cowl region where the shock hits the wall or around the corner where the flow turns from the centerbody spike into the internal compression region of the inlet.

3 Physical Model 3 and Boundary Conditions

To finalize the assessment of inlet flows, a mixed compression inlet specifically designed for Mach 10 flight was considered. It consists of a 18.8º half-angle centerbody spike protruding 0.6827 meter from the cowl lip. The projected frontal area of this inlet is A_i = 0.0929 m^2 (1 ft^2). The width and length of the internal compression passage (constant area region) are

2.44 cm and 50 cm, respectively (see Fig.7). The generic design was taken from Heiser & Pratt.[4] It was optimized for Mach 10: the location of the cowl lip was chosen so that the oblique shocks would reach the lip, and the reflected shock would fall right on the corner between the centerbody and the cowl.

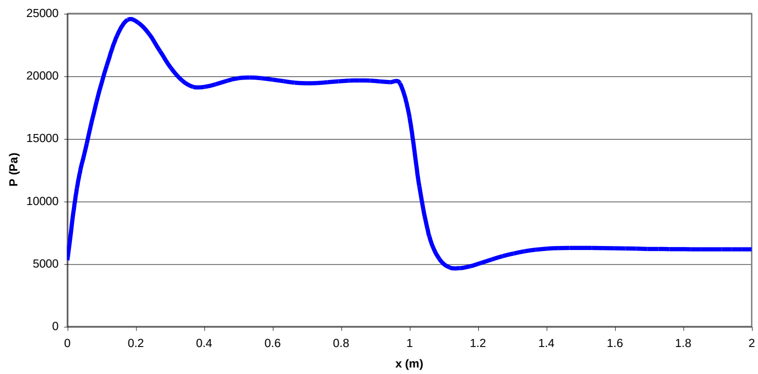

Figure 6. Wall Pressure Distribution – Long Inlet Case 1.

We also analyze the performance of the mixed external-compression inlet at the Mach 10-12 flight conditions. The flow conditions for this study are summarized in Table 2. In order to keep the dynamic pressure at 97.28 kPa (2000 psf), the freestream conditions correspond to an altitude of 29 km for Case 1, and 33 km for Case 2. The two cases assumed viscous turbulent flow. The absolute viscosity of air was calculated with Sutherland's relationship, which is a function of the gas temperature. The axisymmetric form of the Navier-Stokes equations were solved.

A 2-block computational mesh was generated with 121 × 57 and 113 × 57 grid cells, clustered near the solid walls and in the vicinity of the compression surface shoulder where the flow turns into the internal compression region. Because the inlet configuration is symmetric, only one half of the inlet is considered; i.e., half the centerbody spike (compression body) and the upper cowl as shown in Fig. 7.

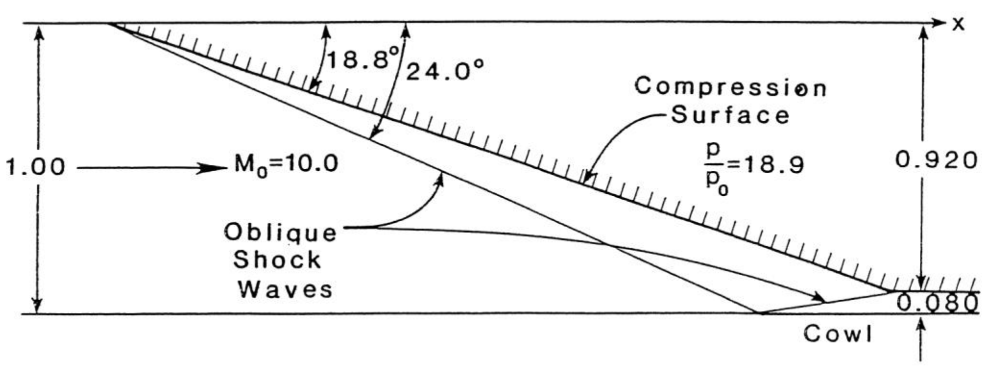

Figure 7. Mach 10 mixed external-internal compression inlet. (Dimensions in ft, Ref. 4).

The inflow boundary was fixed at the free-stream conditions (See Table 2). This condition is representative of a Mach 10 missile scramjet. An extrapolation boundary condition was applied at the exit plane. For viscous flow calculations on solid surfaces, all velocity components (as well as the normal pressure gradient) are required to vanish. A 300 K constant temperature distribution was taken as the thermal boundary condition to be consistent with values reported in the literature. Open boundaries were calculated assuming vanishing normal gradients in velocity, temperature, and pressure.

Table 2. Scramjet Inlet Flow Conditions

CASE	M_∞	T_∞ (K)	P_∞ (Pa)	Re/m	q (kPa)
1	10	225.60	1367.9	4.32 x 10^6	97.27
2	12	227.68	965	3.57 x 10^6	97.27

4 Results

A number of parameters have been formulated for the quantitative evaluation of compression performance systems. For this analysis, we began with adiabatic compression efficiency η_c, as this parameter exerts a profound influence upon overall efficiency of the scramjet engine. As noted in the literature, compression efficiency can "make or break" the performance of an air breathing engine as well as its intended aerospace vehicle.

There are three other standard performance measures that fairly represent engine performance and that can be related to η_c, namely total pressure ratio π_c, kinetic energy efficiency η_{KE}, and dimensionless entropy increase. The following results, extracted from a separate report,[5] will refer to these parameters when assessing the inlet performance at the conditions of interest.

The analysis of the inlet begins by referring to the compression process, the first thermodynamic process in the temperature-entropy (T-s) diagram of a scramjet engine. This represents adiabatic compression from the freestream static temperature T_∞ to the burner entry static temperature T_3. The irreversibilities or "losses" due to skin friction and shock waves cause the entropy to increase from the freestream value s_∞ to the burner entry value s_3. If there were no irreversibilities, no change of entropy would occur, and the adiabatic compression process would be isentropic or ideal.

It is important to note that the static temperature at the end of compression (or beginning of combustion) cannot be increased indefinitely, but must be limited to a value that prevents excessive dissociation in the exhaust flow. The maximum allowable compression temperature T_3 is typically in the range of 1440-1670 K (2600-3000°R). Thus, the entire compression process will take place where the air behaves as a thermally perfect gas with a constant ratio of specific heats γ_c and dissociation effects are negligible.

At the same time, the limit on compression temperature leads directly to restrictions on the burner entry Mach number M_3. From one-dimensional flow energy analysis, the stagnation temperature of the inlet flow can be determined:

$$T_t = T_0\left(1 + \frac{\gamma_c - 1}{2} M_\infty^2\right) = T_3\left(1 + \frac{\gamma_c - 1}{2} M_3^2\right)$$

so that the burner entry Mach number must equal M_3, given by the relation

$$M_3 = \sqrt{\frac{2}{\gamma_c - 1}\left\{\frac{T_\infty}{T_3}\left(1 + \frac{\gamma_c - 1}{2}M_\infty^2\right) - 1\right\}}$$

for the given maximum allowable compression temperature T_3.

Case 1 – Inlet operating at Mach 10.

We begin the assessment of the inlet design with the characterization of the flowfield before its overall performance parameters are determined.

The shocks inside the inlet are represented by the pressure contours showing maxima and minima regions in Fig. 8. The shock train is also manifested in the distribution of wall pressure (Fig. 9) where the pattern after x = 0.9 m represents the decaying strength of the shocks.

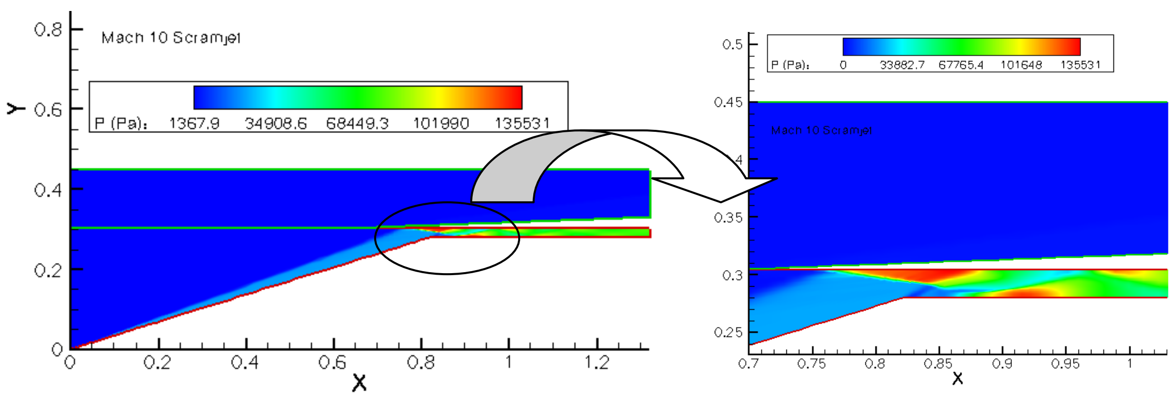

Figure 8. Pressure Contours – Inlet Case 1.

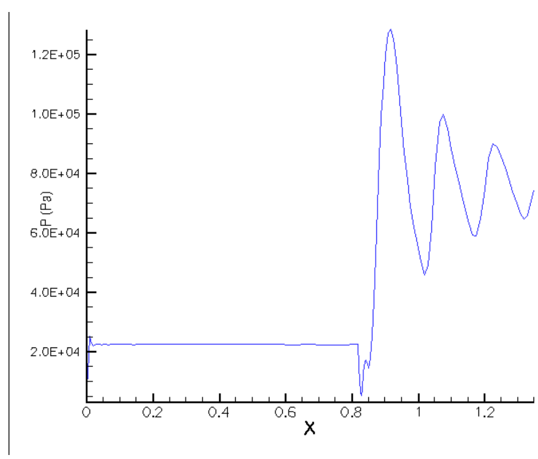

Figure 9. Axial Variation of Lower Wall Pressure – Inlet Case 1.

The flowfield represented by the contours of velocity also give a clue as how well the inlet is performing. As indicated in Fig. 10(a), after the flow turns over the shoulder of the centerbody, the boundary layer tends to separate, a region of recirculation forms as the boundary layer tries to stay attached to the wall. This is where the shock interacts with the boundary layer. As noted in the contour of radial velocity, zooming in Fig. 10(b) to show the region where the flow tries to align itself with the wall, the velocity vector in Fig. 10(c) shows that the boundary separation occurs at x = 0.87 m, but it reattaches immediately downstream This happens because the turbulent boundary layer carries more momentum and thus it overcomes the strong adverse pressure gradients.

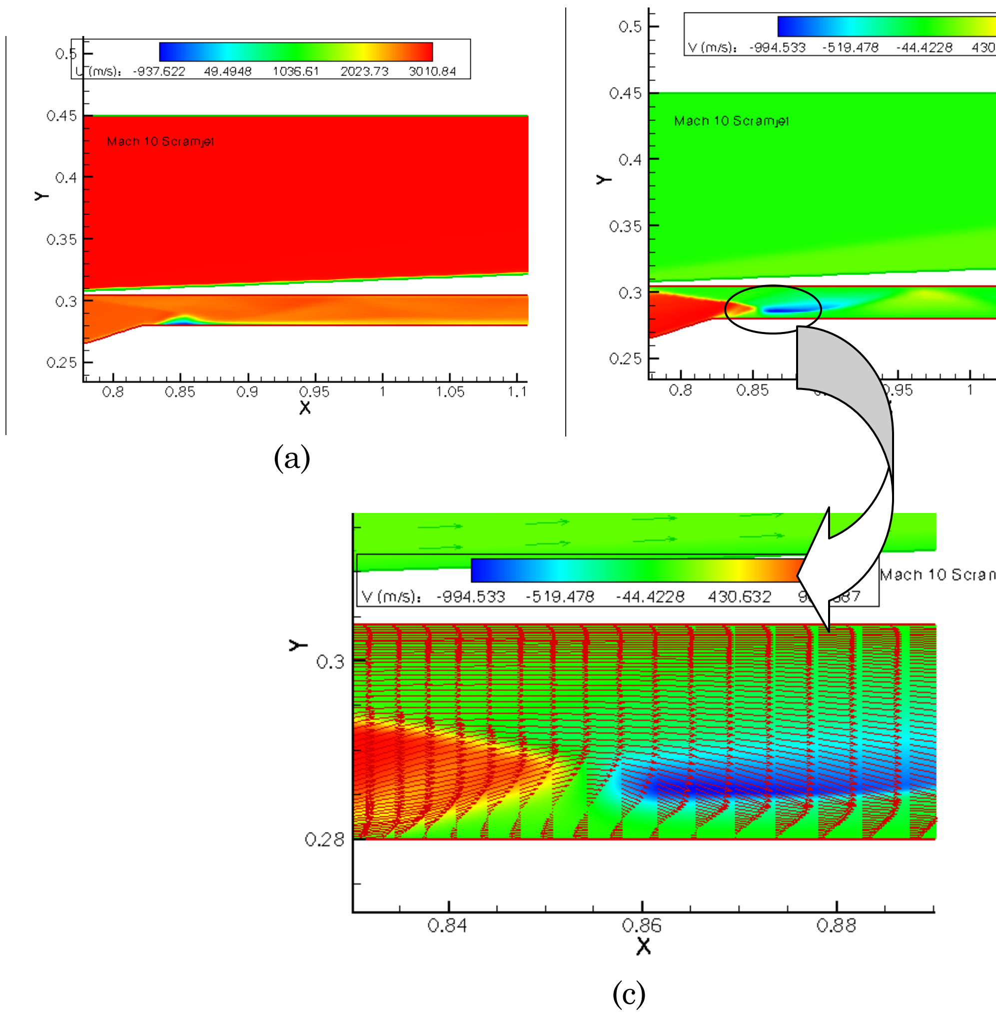

Figure 10. Tangential and Radial Velocity Distribution – Inlet Case 1.

Inlet Performance at Mach 10 Freestream Conditions:

The average air temperature at the end of the compression process (at centerline of exit plane) is 1431.13 K, which is within maximum allowable compression temperature. This gives an engine cycle static temperature ratio $\varphi = T_3/T_\infty = 6.3$, a reasonable value within the typical range of 6-8. The overall compression ratio was calculated as $p_3/p_\infty = 55.72$, resulting from the average air pressure of 76.22 kPa.

The total pressure ratio across the inlet is defined as the ratio of the total pressure at the entrance of the combustor divided by the total pressure of the freestream flow (π_c =

$p_{t3}/p_{t\infty}$) and the compression efficiency, written in terms of total pressure ratio and static temperature ratio is given by,

$$\eta_c = \frac{\varphi - \left(\frac{1}{\pi_c}\right)^{(\gamma_c - 1)/\gamma_c}}{\varphi - 1}$$

With the total pressure ratio $\pi_c = 0.85$, and the static temperature ratio $\varphi = 0.63$, the adiabatic compression of the inlet is $\eta_c = 0.807$.

The kinetic energy efficiency is defined as the ratio of the square of the velocity that the compression component exit flow would achieve if it were isentropically expanded to freestream static pressure to the square of the freestream velocity. With the average velocity at the center of the inlet exit plane, the kinetic energy efficiency for this inlet is calculated as 0.73. Overall, the performance of this inlet is good. No indication of boundary layer separation was observed, even in the cowl region where the shock hits the wall or around the corner where the flow turns from the centerbody spike into the internal compression region of the inlet.

CASE 2. Inlet operating at Mach 12.

Modeling the same inlet at the Mach 12 flow condition is synonymous to simulating a fixed-geometry inlet operating at off-design condition. This is done to understand how the performance is affected.

The first observation comes from the pressure distribution along the wall in Fig. 11. As noted, the first shock is strong enough to compress the air to a value comparable to the compression pressure at Mach 10. However, the strength of the shocks inside the internal compression inlet section drops considerable reaching an average value of 66.45 kPa as the flow exits and would enter the combustion chamber. This represents an overall compression ratio $p_3/p_\infty = 68.85$. The pressure field near the shoulder where the flow turns is given in Fig. 12.

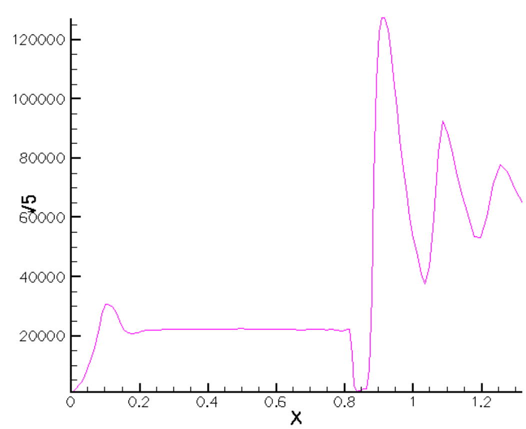

Figure 11. Wall Pressure Distribution – Inlet Case 2.

The Mach number contours are shown in Fig. 13. As expected, when the Mach number increases, the shock angle is smaller, and the distance between the centerbody surface and the shock decreases, causing the shock wave to impinge at a point inside the inlet, missing the lip of the cowl. This is also observed with the pressure contours in Fig. 12.

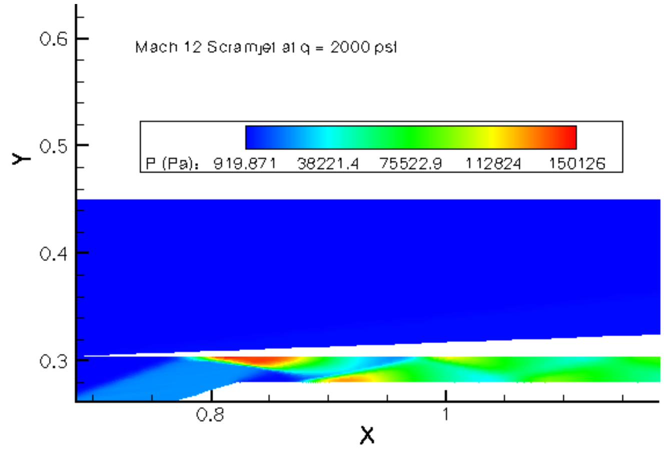

Figure 12. Pressure Contours – Inlet Case 2.

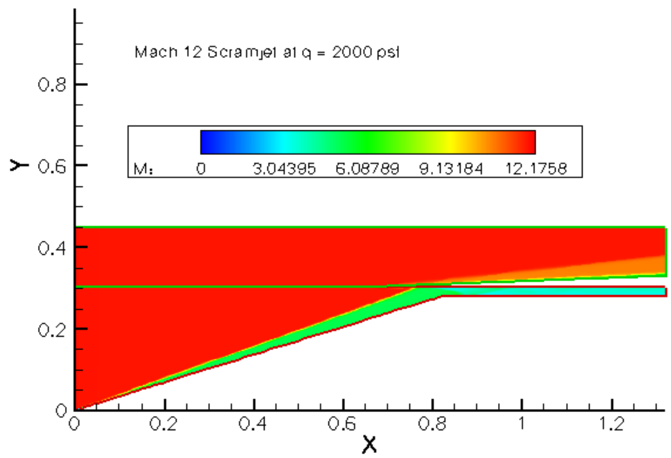

Figure 13. Mach Number Contours – Inlet Case 2.

The low performance of the inlet operating at the off-design Mach 12 condition is also manifested by the large temperature increase of the air as it travels along the internal compression region. At the exit plane of the inlet, the average air temperature reaches a value of 1954 K, but there is a large temperature increase as the gas approaches the upper surface (cowl), reaching values of more than 3000 K. This value exceeds the maximum allowable compression temperature. Figure 14 shows the temperature contours for this case.

With the average velocity at the center of the inlet exit plane, the kinetic energy efficiency for this inlet was calculated as 0.73.

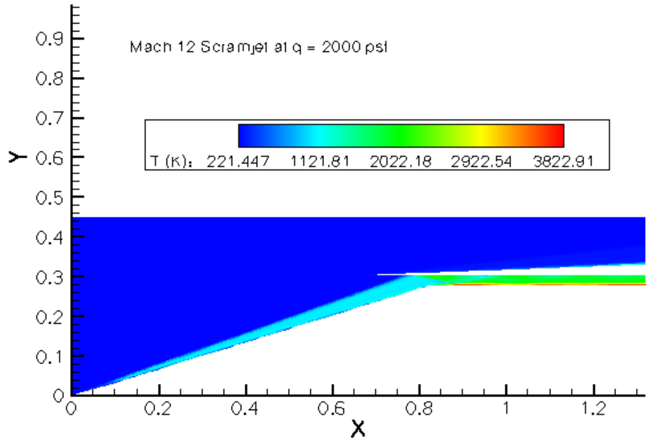

Figure 14. Temperature Contours – Inlet Case 2.

5 Conclusions and Recommendations

The geometry and size of the inlet must be chosen carefully in order to provide the correct flow condition at the entrance of the burner. The inlet design must be optimized for the Mach 10 scramjet missile, before selecting the best location for the upstream fuel injector. This could be positioned on the top surface (cowl), a few centimeters upstream from the shock impingement zone. At that point, the cold fuel would transfer the heat away from the wall and, at the same time should mix with the hot air before entering the combustor and igniting.

Inlets for hypersonic axisymmetric missiles present the ultimate design challenge. The optimum geometry corresponds to the well-known shock-on-lip (SOL) condition illustrated in Fig. 15: the compression ramp shocks converge on the cowl lip, and the reflected shock impinges on the upper boundary of the inlet. Since shock angles are determined by the flight Mach number, the SOL condition cannot be met at Mach numbers higher or lower than the design Mach number. At Mach numbers higher than the inlet design Mach number, the shocks move inside the inlet (Fig. 16), causing multiple reflected shocks, loss of stagnation pressure, possible boundary layer separation, and engine unstart. At Mach numbers lower than the design Mach number, the so-called spillage occurs, and the air mass capture decreases (Fig. 17).

To avoid performance penalties at off-design Mach numbers, a variable geometry inlet can be used. However, the mechanical variable geometry system would add weight and complexity to the design. Thus, an alternative approach is to optimize the inlet using energy addition to or extraction from the flow. Plasmas and various magnetohydrodynamic (MHD) devices have been proposed to optimize scramjet inlets.

We continue developing new innovative approaches to design and engineer inlet components for very high-speed vehicles (M > 8). This includes computational fluid dynamics (CFD) modeling and simulation methodologies. CFD models should be able to accurately simulate the physics of strong shock interactions, incident oblique shocks, compression corners and shock expansions. Moreover, these models must include multiple air injection paths to control shockwave-boundary layer interaction, as well as complex flow spillages.

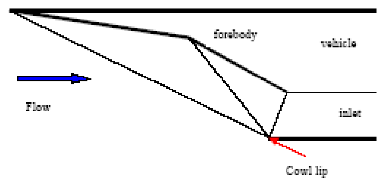

Figure 15. Design forebody and inlet geometry with shock-on-lip (SOL) condition.

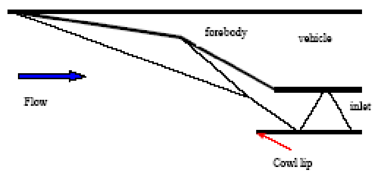

Figure 16. Flow and shock geometry at Mach number higher than the design one.

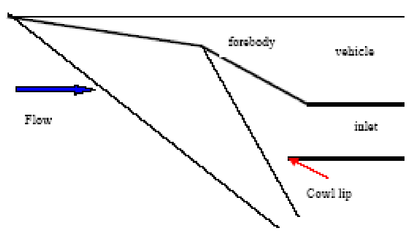

Figure 17. Flow and shock geometry at Mach number lower than the design one.

Air inlet designs should be optimized for hypersonic cruise operation. Design optimization is a function of the Mach number: as Mach number increases, lip cowl drag is more important while bleed, spillage drag and bypass flow are emphasized less. The emphasis is on achieving low off-design drag and flow matching for stability (unstart-free) and integration of the variable cycle power plants. Efficient integration of the inlet with airframe is also critical in this speed regime and the optimization of the inlet design can be achieved both at the component and system level.

As a follow-up study we propose to do the following:

- Continue to develop design procedures employing the CFD methodologies. This requires to further improve the selected models so that they can be employed/validated in prototype demonstration. Demonstrate accurate performance analysis of very high-speed inlets with quick turn-around times.
- Successful development of the improved CFD methodologies for high-speed inlets should enable design engineers to select new and innovative concepts that optimize inlet performance and to integrate these designs in future high-speed air vehicles in a very cost-efficient manner.
- Of primary interest are the accuracy of the simulations compared to experimental data, as well as the practicality of the simulations in terms of turn-around times.

Applicability of these methodologies in the design process for high-speed inlets must be demonstrated.

References

[1] Musielak, D.E., “Numerical Simulation of Flow Development in a Scramjet Inlet.” Progress Report for the Scramjet Development Program: Report No. 2, March 2006.

[2] Musielak, D.E., “Modeling of Mach 10 Scramjet Inlet Flow and Assessment of Injector Location,” Progress Report for the Scramjet Development Program, August 2006.

[3] Musielak, D.E., “CFD Study of a Mach 10-12 Scramjet,” Final Report for the Scramjet Development Program, April 2007.

[4] Heiser W.H., and Pratt, D.T., *Hypersonic Airbreathing Propulsion*, AIAA Education Series, 1994.

[5] Musielak, D.E., “Mach 10-12 Scramjet Inlet Performance Assessment.” Scramjet Development Program, Contractor Report No. 8, September 2006.